DYNAMIC RECRYSTALLIZATION IN HIGH-STRAIN, HIGH-STRAIN-RATE PLASTIC DEFORMATION OF COPPER

U. ANDRADE, M. A. MEYERS, K. S. VECCHIO and A. H. CHOKSHI

Department of Applied Mechanics and Engineering Science, University of California, San Diego,
La Jolla, CA 92093-0411, U.S.A.

Abstract—When copper is deformed to high plastic strain ($\gamma \sim$ 3–4) at high strain rates ($\dot{\gamma} \sim 10^4\,\text{s}^{-1}$) a microstructure with grain sizes of $\sim 0.1\,\mu\text{m}$ can be produced. It is proposed that this microstructure develops by dynamic recrystallization, which is enabled by the adiabatic temperature rise. By shock-loading the material, and thereby increasing its flow stress, the propensity for dynamic recrystallization can be enhanced. The grain size–flow stress relationship observed after cessation of plastic deformation is consistent with the general formulation proposed by Derby [*Acta metall. mater.* **39**, 955 (1991)]. The temperatures reached by the specimens during dynamic deformation are calculated from a constitutive equation and are found to be, for the shock-loaded material, in the 500–800 K range; these temperatures are consistent with static annealing experiments on shock-loaded specimens, that show the onset of static recrystallization at 523 K. A possible recrystallization mechanism is described and its effect on the mechanical response of copper is discussed.

1. INTRODUCTION

Plastic deformation at low plastic strains (0–0.5) is well described by simple dislocation theory; Taylor [1], Seeger [2], Hirsch [3] and Kuhlmann-Wilsdorf [4] developed fully quantitative theories that predict the parabolic stress–strain response. At higher plastic strains ($>$ 1), complex dislocation interactions with the formation of sub-grains, inhomogeneities, and other peculiarities ensue; the review by Sevillano *et al.* [5] illustrates these complexities. Brown [6] refers to this as Stage IV and indicates that it can, in many instances, lead to tensile instabilities. At high strain rates, the process is essentially adiabatic, and at large plastic strains, the thermal excursion associated with plastic deformation can be significant. Most high-strain-rate research has focused on low plastic strains, and the constitutive models proposed (e.g. Harding [7], Follansbee and Kocks [8], Zerilli and Armstrong [9]) are based on dislocations overcoming obstacles by thermal activation. A preliminary investigation of high strain rate deformation in copper indicated the possibility of dynamic recrystallization during high strain, high strain rate deformation [10].

This paper represents a first attempt to extend the plastic strain into a regime in which recovery/recrystallization processes can occur in concomitance with plastic deformation. This regime is of great technological importance, since many applications (e.g. shaped charges, explosively-forged projectiles, armor defeat, explosive welding and explosive compaction) involve plastic strains in excess of 1.

Copper was used in these experiments because its high-strain-rate response has been extensively studied

in the literature and it possesses good ductility. In order to enhance the thermal energy generation per unit plastic strain, the flow stress of the copper was increased by subjecting it to a pre-deformation shock loading treatment.

2. EXPERIMENTAL APPROACH

The setup used to shock harden the copper specimens has been described previously [11]. A flyer plate (4.7 mm thick stainless steel) was accelerated to a velocity of 2.1 km/s by an explosive (PBX 9501). The explosive is initiated by a plane wave generator (explosive lens) which is initiated, on its turn, by a detonator placed at the top. The impact velocity of 2.1 km/s generated a pressure within the copper specimen of 50 GPa. The impact velocity was measured by means of contact pins. Three contact pins were used, connected to a transient recorder. The recorded velocities, at three positions, were 2.07, 2.1, and 2.13 km/s. The state of stress generated by shock loading is not hydrostatic, but one of uniaxial strain, and significant shear strain components exist both at the front and release portions of the stress pulse. Using data for copper from Meyers and Murr [12] and uniaxial strain, ϵ_x, produced by the shock wave can be calculated by

$$\epsilon_x = \ln \frac{V}{V_0} \tag{1}$$

where V and V_0 are the compressed (obtained through the equation of state) and initial specific volumes for copper, respectively. Taking the strains at the shock front and release portion to be the same

(but with opposite senses, yielding a zero residual strain), then the total strain, ϵ_{xT}, is given by

$$\epsilon_{xT} = 2 \ln \frac{V}{V_0}. \tag{2}$$

An effective plastic strain can therefore be computed for the uniaxial strain state ($\epsilon_y = \epsilon_z = 0$) by

$$\epsilon_{\text{eff}} = \frac{\sqrt{2}}{3} [(\epsilon_x - \epsilon_y)^2 + (\epsilon_x - \epsilon_z)^2 + (\epsilon_y - \epsilon_z)^2]^{1/2}$$

$$= \frac{2}{3} \epsilon_x \tag{3}$$

from which the total transient plastic strain, $\epsilon_{\text{eff}-T}$, for the forward and reverse directions is

$$\epsilon_{\text{eff}-T} = \frac{2}{3} \left(2 \ln \frac{V}{V_0} \right) = \frac{4}{3} \ln \frac{V}{V_0}. \tag{4}$$

At an impact velocity of 2.1 km/s, a shock pressure of 50 GPa is created, yielding $V/V_0 = 0.813$ and an effective transient strain of 0.276. The measured residual plastic strain was equal to ~ 0.05, validating the assumption of equation (2). Care was taken to minimize the residual strain, since it has been shown by Mogilevsky and Teplyakova [13] and Gray [14] that it has a marked effect on the deformation
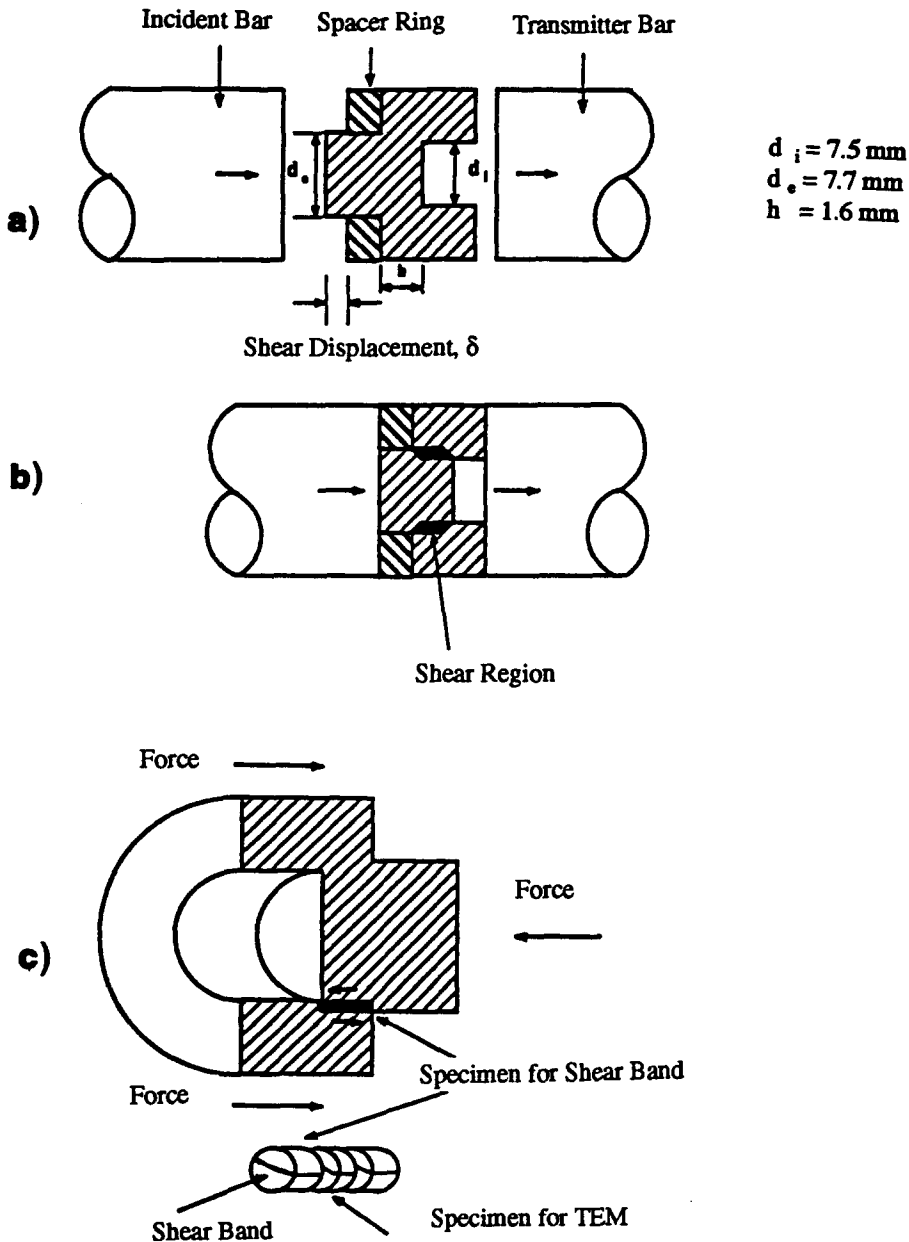

Fig. 1. Scheme of loading the hat-shaped specimen in the Hopkinson bar: (a) specimen before compression; (b) specimen after compression; (c) extraction of specimen for transmission electron microscopy.

microstructure and on the resultant strengthening. A lateral momentum trap was employed to trap the lateral release waves, and a bottom momentum trap to prevent spalling of the copper plate. The procedures for recovery fixture design are well known and are described by De Carli and Meyers [15] and Gray [16], among others. The copper plate had a mean linear intercept grain size of 70 μm.

Mechanical tests were performed at quasi-static and dynamic strain rates using cylindrical and hat-shaped specimens. Cylindrical specimens were used for quasi-static compression tests (6 mm diameter, 6 mm length) and dynamic compression tests (6 mm diameter, 3.6 mm length). Hat-shaped specimens were used to generate high strain, high-strain-rate deformation under controlled, prescribed conditions. The hat-shaped specimen geometry was developed by Meyer and co-workers [17] and is shown in Fig. 1. The specimen has a circular cross-section and its longitudinal section is shown in Fig. 1(a). The displacement, δ, is established by the thickness of a high-strength steel ring acting as a stopper (spacer ring in Fig. 1). The hat-shaped specimen is placed between the incident and transmitter bars of a split Hopkinson (Kolsky) bar. After plastic deformation,

the distance δ is reduced to zero and the configuration shown in Fig. 1(b) is reached. A concentration region of plastic deformation under conditions close to pure shear is established, and the shear stress generated is approximately equal to

$$\tau = \frac{P}{\pi h \left(\dfrac{d_i + d_e}{2} \right)}. \qquad (5)$$

The shear strain is equal to the displacement δ divided by the thickness of the shear region, t

$$\gamma = \frac{\delta}{t}. \qquad (6)$$

The shear stress and strain can be converted into normal stress and longitudinal strain by the expression

$$\sigma = 2\tau$$

$$\epsilon = \ln\left(\frac{\gamma^2}{2} + \gamma + 1 \right)^{1/2}. \qquad (7)$$

Specimens for transmission electron microscopy (TEM) were obtained by trepanning, by electrical discharge machining, 3 mm diameter cylinders, oriented as shown in Fig. 1(c). These cylinders were then
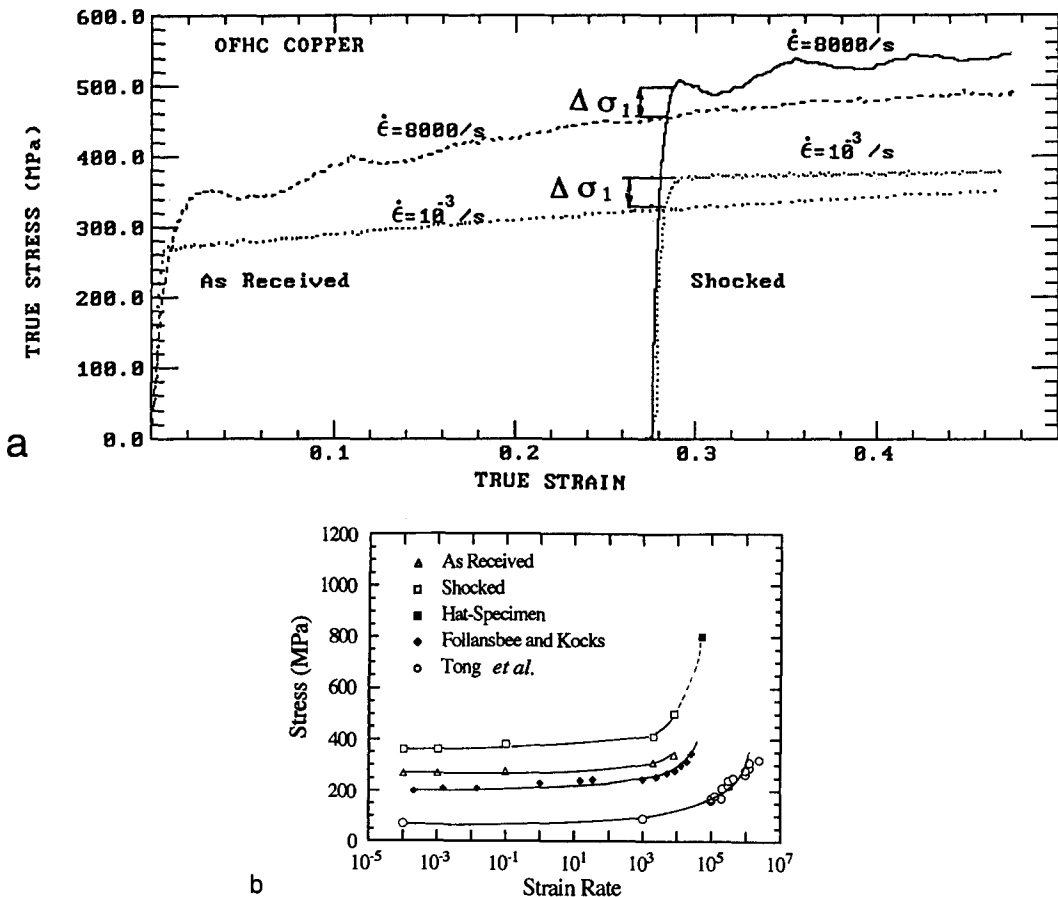

Fig. 2. (a) Compressive stress–strain response of as-received and shock-loaded copper at strain rates of 10^{-3} and $8 \times 10^3 \, \text{s}^{-1}$; prestrain of 0.276 established as origin for shocked material. (b) Flow stress (at 1% plastic strain) as a function of strain rate for the as-received and shocked conditions.

sectioned into disks (~1 mm thick) with the central region used for transmission electron microscopy. After hand-grinding the disks down to 0.2 mm, TEM foils were electropolished to perforation in a solution of 60% orthophosphoric acid and 40% water. In some cases, further thinning was performed by cold ion-milling in order to ensure electron transparency in the region containing the shear band. TEM observations were made in a Philips CM30 transmission electron microscope operating at 300 kV.

3. RESULTS AND DISCUSSION

3.1. Mechanical tests

The effect of shock loading on the strength of the copper specimens is illustrated in Fig. 2, which shows both the low (10^{-3}s^{-1}) and high $(8 \times 10^3 \text{s}^{-1})$ strain-rate responses of as-received and shock-loaded materials. The as-received material had been rolled to a 25% reduction in thickness and therefore its yield stress (~260 MPa) is higher than annealed copper

Fig. 3. (a) Optical micrograph of shock-loaded copper, with arrows indicating intertwin spacings; (b–c) optical micrographs of shear deformation regions for as-received and shock-loaded copper, respectively, deformed to the same plastic strain of $\gamma = 2$.

with the same grain size (~140 MPa). The effect of shock loading is well documented in the literature; De Angelis and Cohen [18, 19] found that there is a threshold pressure for twinning in copper, equal to 14 GPa for single crystals in the [100] orientation and 20 GPa in the [111] orientation; Murr [20] reported a threshold pressure of 20 GPa for polycrystalline copper. Gray and Follansbee [21] studied the effect of pulse duration and peak pressure on the shock response of copper. The mechanical response of the shocked copper displayed in Fig. 2(a) is consistent with these earlier studies. The flow stress is increased from 260 to 340 MPa, whereas the work hardening decreases. The effect of shock was accounted for by translating the origin to the right by the value $\epsilon = 0.276$. At a strain of 0.276, the strength level achieved by shock loading is greater than the strength level normally achieved due to normal work hardening at low strain rates. Mechanical twinning is the main contributor for the enhanced strengthening in shock loading, due to the reduced dislocation barrier spacing. The increase in strength due to shock loading relative to the normal work hardened strength, $\Delta\sigma_1$ [see Fig. 2(a)], can be interpreted in terms of the decrease in the effective grain size due to the formation of the deformation twins. The profuse twinning produced by shock loading seen in Fig. 3(a) produced an inter-twin spacing equal to ~5–10 μm. Applying the Hall–Petch relationship

$$\Delta\sigma = k(d_1^{-1/2} - d_2^{-1/2}) \tag{8}$$

to the inter-twin spacing in the shock-loaded material, d_1, and its initial grain size, d_2, the increased strengthening can be calculated. For copper, the reported values for k vary between 1.58×10^{-4} and $3.5 \times 10^{-4} \text{ GPa m}^{1/2}$: {Feltham and Meakin [22]: 3.53×10^{-4}; Gourdin and Lassila [23]: 2.78×10^{-4}; Zerilli and Armstrong [9]: 1.58×10^{-4}; Andrade [24]: $2.60 \times 10^{-4} \text{ GPa m}^{1/2}$.} Using 1.58×10^{-4} and 3.5×10^{-4} as lower and upper bounds, respectively, the increased strengthening, $\Delta\sigma$, ranges from 20 to 45 MPa. This increase is entirely consistent with $\Delta\sigma_1$ [shown in Fig. 2(a)] which is approx. 40 MPa. This analysis suggests that twin boundaries produced by shock-loading copper can act as effective obstacles to dislocation motion.

The flow stress of as-received and shock-loaded copper as a function of strain rate is given in Fig. 2(b). The high-strain-rate experiments were carried out in a split Hopkinson bar, whereas the quasi-static experiments ($\dot{\epsilon} \leqslant 10^{-1} \text{s}^{-1}$) were carried out in a uniaxial servohydraulic machine. The strain-rate sensitivity of copper is apparent from the experimental results. The results obtained are entirely consistent with those reported by Follansbee and Kocks [8] and Clifton and co-workers [26, 27]; their material was in the annealed condition, and therefore their curve is translated downwards toward a lower stress for a given strain rate. The four curves are
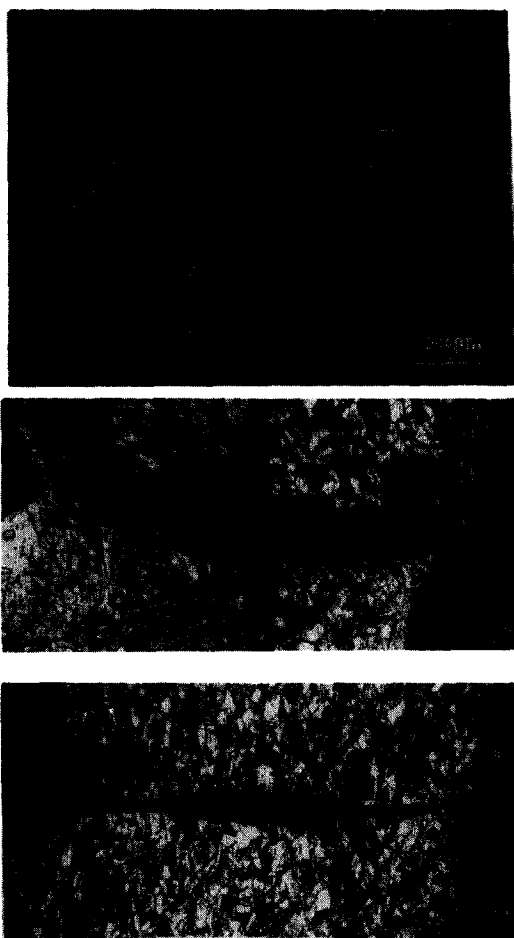
approximately parallel, and the strain-rate sensitivity shows a marked increase beyond $10^4\,\text{s}^{-1}$. This has been interpreted by Follansbee and Kocks [8] and Tong *et al.* [27] as due to a change in the rate of dislocation generation. One single data point, for a strain rate of $5 \times 10^4\,\text{s}^{-1}$, is reported in Fig. 2(b) for the hat-shaped specimen.

Figure 3(b, c) shows the shear localization regions resulting from plastic deformation at high strain rate of the hat-shaped specimens. The as-received copper specimen [Fig. 3(b)] shows a more diffuse plastic deformation region, whereas the shock-loaded specimen shows a clearly defined shear region [Fig. 3(c)]. The greater localization of the shock-loaded condition will be discussed later.

The strain rate within the plastic deformation region of the hat-shaped specimens can be estimated from the velocity of the interface between the incident bar and specimen. This velocity, v, divided by the thickness, t, of the plastic deformation region, provides the shear strain rate

$$\dot{\gamma} = \frac{v}{t}. \tag{9}$$

For a velocity of 8 m/s (equal to the impact velocity of striker bar on the incident bar) and an estimated thickness of the plastic deformation region of $\sim 200\,\mu\text{m}$ [from Fig. 3(b, c)] a shear strain rate equal to $4 \times 10^4\,\text{s}^{-1}$ is calculated. An independent verification was obtained by the stress vs time records, which yielded the total time over which plastic deformation occurred.

Different shear strain, γ, were obtained by varying the magnitude of the displacements, δ [as depicted in Fig. 1(a)]; values of δ equal to 0.4, 0.5, 0.75, 1.0, and 1.4 mm, were prescribed. In addition, the plastic shear strain can be estimated from the slope of the distorted flow lines in the plastic deformation region
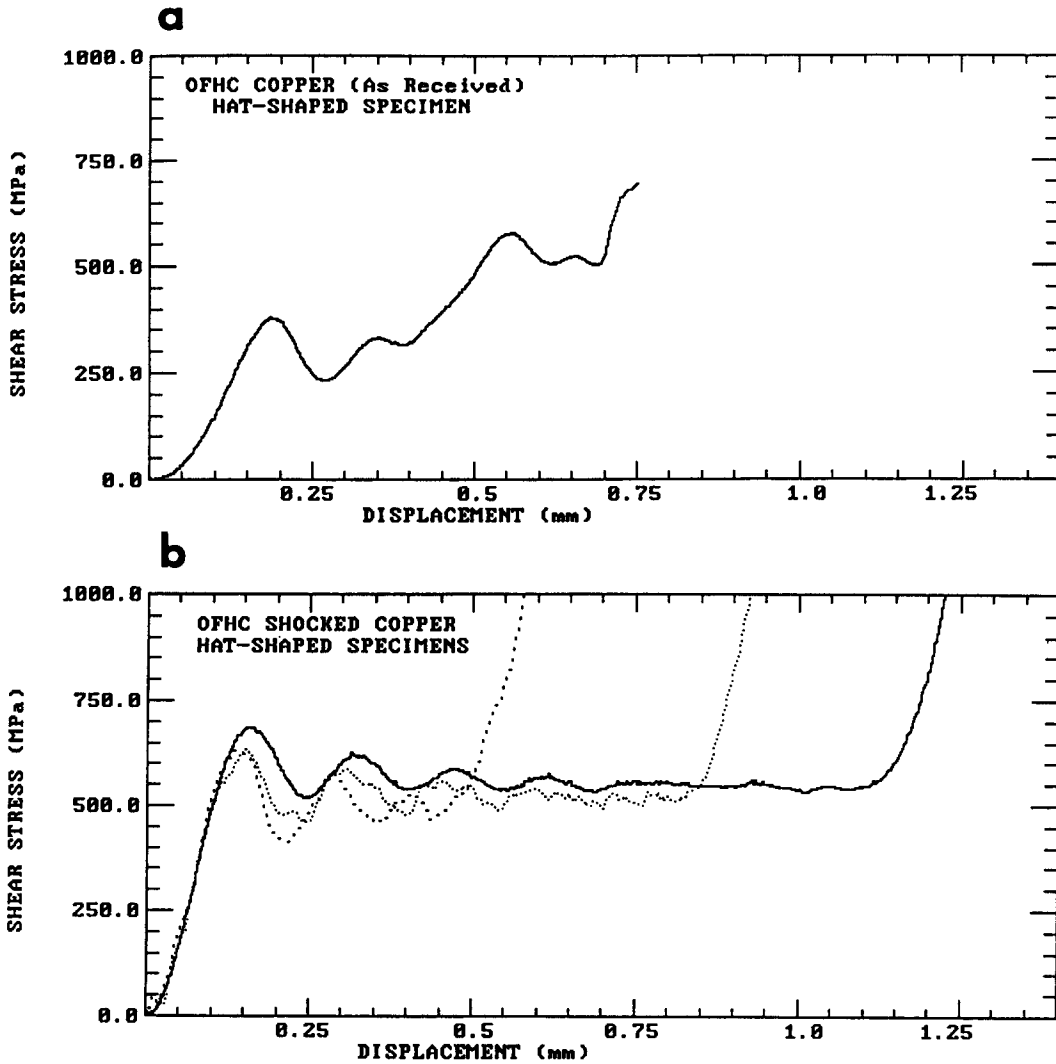

Fig. 4. Shear stress vs displacement curves for hat-shaped specimens: (a) as-received material; (b) shock-loaded material with different prescribed displacements of δ of ~ 0.4, 0.75 and 1.4 mm. Notice the upturn of the curves when prescribed displacement is reached.

relative to the loading direction. The thickness of the band, t, shows a distinct increase with shear strain, and the microstructural features within these bands cannot be clearly resolved with the metallograph. The shear stress vs displacement curves for the different specimens are shown in Fig. 4. These curves exhibit oscillations due to reflection of waves at the specimen surfaces and stopper rings. The as-received material shows work-hardening [Fig. 4(a)], whereas the shock-loaded materials show relatively flat shear stress–displacement curves. The shear flow stresses are consistent for the three experiments and equal to ~ 550 MPa; this yields a normal stress of ~ 1100 MPa. A correction was introduced to account for the deviation from pure shear, for the possible anisotropy of flow stress of specimens, and for the stress concentrations. This correction was made on the basis of low-strain-rate compressive tests, from which a conversion factor of 0.75 was derived. This brings the value of 1100 MPa down to 800 MPa. This result is plotted in Fig. 2(b), and a dashed line was drawn, indicating uncertainty because of a change in testing technique. Nevertheless, the isolated datum is consistent with the flow stress upturn reported by Follansbee and Kocks [8] and pressure-shear experiments carried out by Clifton and co-workers [26, 27].

Fig. 6. Break-down of the elongated cells resulting in the formation of sub-grains.

Fig. 5. Transmission electron micrographs of the shear region in specimen subjected to shear strain of 2: (a) elongated cells inside the shear band; (b) elongated cells at higher magnification.

3.2. Transmission electron microscopy

The microstructure within the shear region of Fig. 3(c) was characterized by transmission electron microscopy, the specimens being sectioned as shown in Fig. 1(c). [It is important to point out that the orientation of the shear band in the TEM specimen is such that the direction of shear was "in and out" of the foil thickness.] Individual grains cannot be resolved optically for $\gamma \geqslant 2.5$. Thus, the specimen with $\gamma = 2$ was analyzed to identify the structures present at initiation of the localization of plastic deformation. Elongated cells with a width of ~ 0.1 μm are evident in Fig. 5; these elongated cells occur in pockets and have also been observed recently by Liu and Bassim [28]. Within these cells, a structural breakdown occurs in certain regions forming sub-grains, as shown in Fig. 6. These features, incipient at $\gamma = 2$, become the main characteristic within the shear localization region at a shear strain > 2.5.

The sequence of transmission electron micrographs shown in Fig. 7 demonstrates how the shock-induced microstructure (dislocations and mechanical twins) is replaced by a microcrystalline structure in the regions adjacent to, and in the center of, the shear localization regions. Figure 7(a) shows the microstructure of the dislocation networks characteristic of shock hardening. At the region adjacent to the plastic shear band, elongated cells with more clearly defined boundaries replace the equiaxed cells [Fig. 7(b)]. Since the foil plane is perpendicular to the direction of plastic deformation, the third dimension of these cells is not seen. They are expected to be "pancake" shaped. As the center of the plastic deformation region is approached, the elongated cells break down and are replaced by equiaxed grains, with a fairly low dislocation density. The boundaries between these small (~ 0.1 μm) grains are well defined, and the

diffraction patterns of Fig. 7(c, d) show that there is a nearly continuous distribution of orientations, with the greatest distribution of orientations occurring at the center of the shear band. Therefore, the angles between individual grains are expected to be larger than 6°. There is a clear trend of increased recrystallization with strain, which increases from the edge of the shear band and reaches a maximum at the center. The evolution of the microstructure leading to this microcrystalline structure is discussed in Section 3.4.
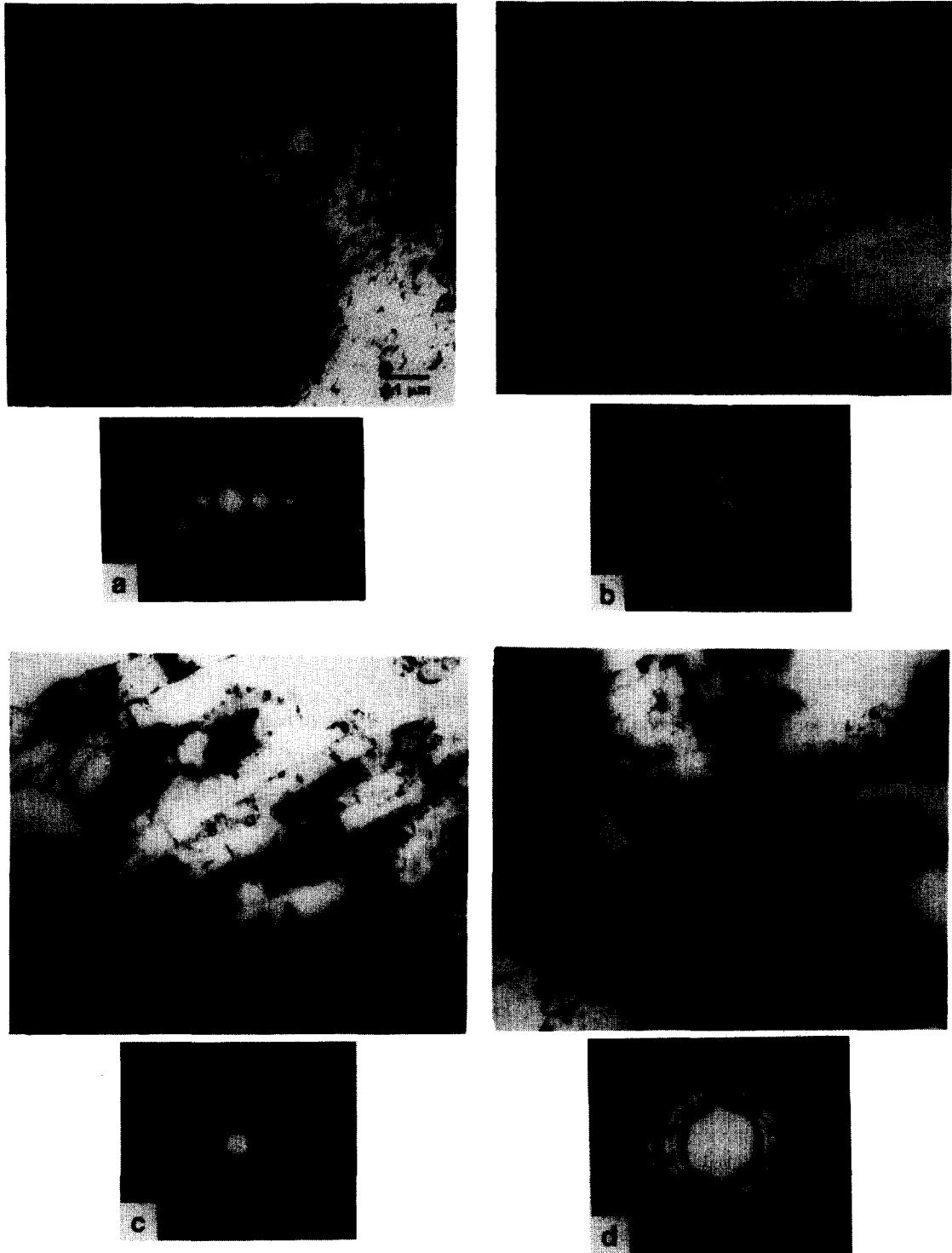
Fig. 7. Tranmission electron micrographs and diffraction patterns from specimen subjected to shear strain of 5: (a) region outside shear localization area; (b) region adjacent to shear localization area; (c) region at onset of shear localization area; (d) region at center of shear localization area.

3.3. Constitutive description

The temperature evolution within the high shear region can be calculated, assuming a constitutive equation that describes the response of both as-received and shock-loaded copper. Several constitutive equations have been developed to describe the high-strain-rate response of metals: Follansbee and Kocks [8], Harding [7], Zerilli and Armstrong [9], and Klepaczko [30] models have under-pinnings in the physical processes occuring in metals during plastic deformation (thermally-activated dislocation motion), whereas the Johnson and Cook [31] model is phenomenological. The Johnson–Cook model was applied to the experimental results and enabled the prediction of temperature as a function of plastic strain, as well as an instability strain. The equation has the form

$$\sigma (\sigma_0 + B\epsilon^n)\left(1 + C \log \frac{\dot{\epsilon}}{\dot{\epsilon}_0}\right)\left[1 - \left(\frac{T - T_r}{T_m - T_r}\right)^m\right] \quad (10)$$

where σ_0, B, n, C, and m are parameters determined experimentally; T, T_r, and T_m are the current, reference (initial: 298 K) and melting (1356 K) temperatures, respectively; $\dot{\epsilon}_0$ is the reference strain rate; σ and ϵ are the stress and strain, respectively. By defining

$$T^* = \frac{T - T_r}{T_m - T_r} \quad (11)$$

and by incorporating the work of deformation into an (adiabatic) temperature rise

$$dT = \frac{0.9}{\rho C_p} \sigma \, d\epsilon \quad (12)$$

a relationship between the temperature and plastic strain, at a fixed strain rate, can be written as

$$T^* = 1 - \exp\left[\frac{-0.9(1 + C \log \dot{\epsilon}/\dot{\epsilon}_0)}{\rho C_p(T_m - T_r)}\right.$$
$$\left. \times \left(\sigma_0\epsilon + \frac{B\epsilon^{n+1}}{n+1}\right)\right]. \quad (13)$$

The instability strain can likewise be obtained by setting

$$\frac{d\sigma}{d\epsilon} = 0. \quad (14)$$

This leads to

$$\frac{(\sigma_0 + B\epsilon^n)^2}{nB\epsilon^{n-1}} = \frac{\rho C_p(T_m - T_r)}{0.9\left(1 + C \log \frac{\dot{\epsilon}}{\dot{\epsilon}_0}\right)}. \quad (15)$$

The parameters σ_0, B, and n, are taken from the experimental results on cylindrical specimens and displayed in Fig. 2(a). The following parameters were established, at a strain rate of $10^{-3} \, s^{-1}$ (taken as the reference strain rate):

as-received (AR)	shock-loaded(SL)
$\sigma_0 = 225$MPa	$\sigma_0 = 330$ MPa
$B = 178$ MPa	$B = 53.7$ MPa
$n = 0.67$	$n = 0.56$

The value of C is the slope of the logarithmic plots of Fig. 2(b). The Johnson–Cook model does not account for the upturn in flow stress beyond $10^4 \, s^{-1}$; these values are approximately: $C_{AR} = 0.027$ and $C_{SL} = 0.026$. The thermal softening parameter, m, was obtained experimentally, and this requires tests at different temperatures. Johnson and Cook [31] report a value for m of 1.04 for copper and this was approximated as 1 for the computations reported herein. The flow stresses at 1% plastic strain for the shocked and as-received conditions are plotted in Fig. 8(a). A best fit for a linear plot of $\log[1 - \sigma/(\sigma_0 + B\epsilon^n)(1 + C \log \dot{\epsilon}/\dot{\epsilon}_0)]$ vs $\log T^*$ provides values of $m = 0.97$ and 1.00 for the as-received and shocked conditions, respectively. The marked decreases in flow stress observed at 570 and 650 K for the shocked and as-received conditions wil be discussed in Section 3.4.
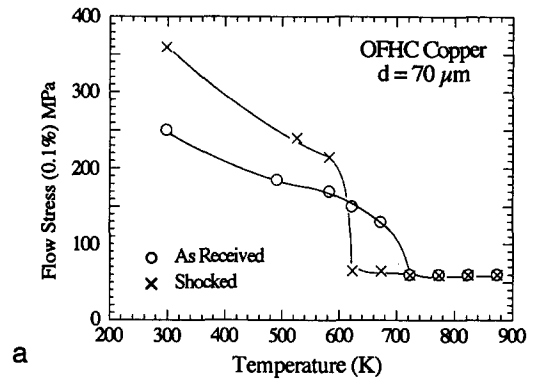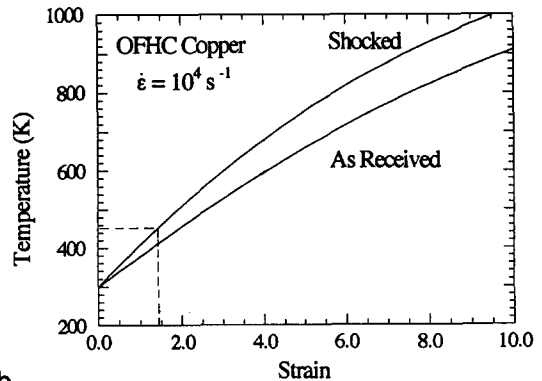
Fig. 8. (a) Flow stress vs temperature for as-received and shocked conditions. (b) Variation in the temperature with plastic strain during dynamic adiabatic deformation at strain rate of $10^4 \, s^{-1}$ and initial temperature of 298 K.

The application of these parameters to equation (13) yields the temperature evolution curves shown in Fig. 8(b). The shocked material exhibits a more rapid temperature rise than the as-received condition, due to the higher flow stress. The range of shear strains at which the microstructure is radically altered, resulting in small grains ($\sim 0.1\ \mu$m) is, for the shock-loaded material, $\gamma = 3 \rightarrow 4$. By applying equation (7) these shear strains can be converted into longitudinal strains; this strain range is indicated by the dotted vertical lines in Fig. 8(b). The predicted temperature reached in the shock-loaded material is 450 K for $\gamma = 4$.

It is also possible to calculate an instability strain, although the curves shown in Fig. 4 do not exhibit any drop that would signify softening. The require-

ment for instability is: $d\sigma/d\epsilon \leqslant 0$. By applying equation (15) and using the parameters obtained experimentally, the following values for the instability strains are obtained:

as-received: $\epsilon_{inst} = 2.2$

shocked: $\epsilon_{inst} = 0.42$.

These values can be converted into shear strains by the application of equation (7)

as-received: $\gamma_{inst} = 11.4$

shocked: $\gamma_{inst} = 0.90$.

These predictions are only in qualitative agreement with the experiments. However, these results indicate that it is virtually impossible to creat an instability
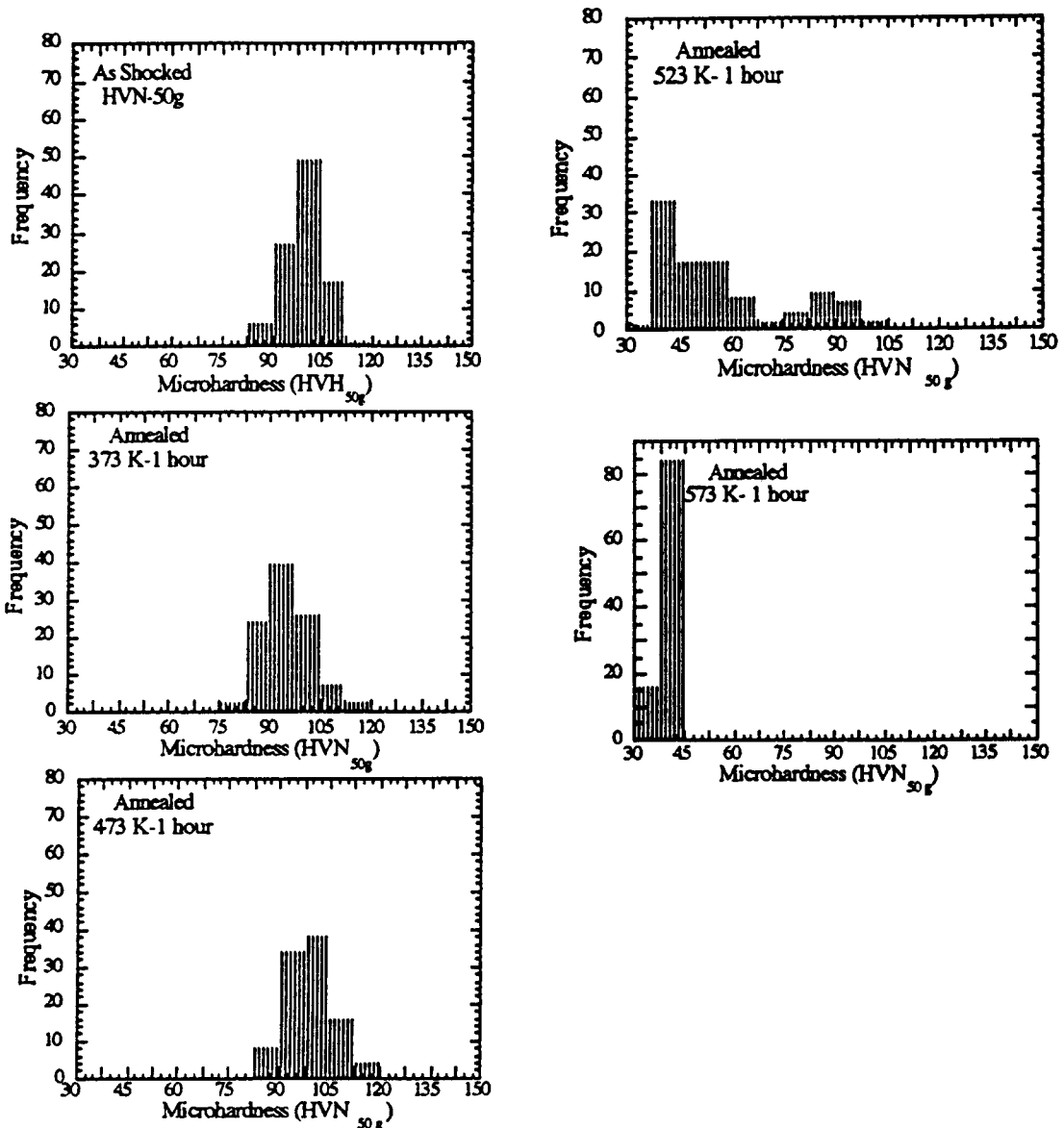

Fig. 9. Microindentation hardness measurements on specimens shock-loaded and subjected to 1 h annealing treatments at the temperatures indicated.

(shear band) with the as-received copper, although the shock-load copper localizes readily. The clear boundary between the plastic shear and undeformed regions in Fig. 3(c) is an indication that localization is taking place. In contrast, the diffuse plastic deformation region for the as-received material [Fig. 3(b)] indicates that this condition is not conductive to localization.

3.4. Proposed mechanism for microstructral evolution

The microcrystalline structure observed within the intense plastic deformation region as well as the temperatures reached within that region (~ 500 K) indicate that recrystallization is the most probable mechanism for the microstructral alteration. The temperatures that mark the onset of thermal recovery/recrystallization processes in metals are generally

$$T = (0.4 - 0.5)T_m.$$

Thus, for copper, $T = (542 - 678)$K; the temperatures predicted for the shear region shown in Fig. 8 fall into this range, making these mechanisms viable. Isochronal (1 h) annealing experiments were conducted on shock-loaded specimens, followed by microhardness measurements. These microhardness measurements were made with a very low load (30 g) in order to produce indentations of such a size that individual recrystallized regions could be probed. These experiments were patterned after earlier research by Chojnowski and Cahn [32]. These measurements are shown in Fig. 9, and are consistent with the constitutive equation calculations: softening, indicative of static recrystallization, occurs at 532 K. Thus, 523 K, the temperature at which the recrystallization (static or dynamic) takes place, is $\sim 0.4\, T_m$.

The quesion of whether these recovery processes occur during or after plastic deformation can be addressed by establishing the time for plastic deformation region, t_{PD}, as: $t_{PD} = \delta/v$, where δ is the distance in Fig. 1(a), and v is the velocity of the incident bar. For $\gamma = 4.5$

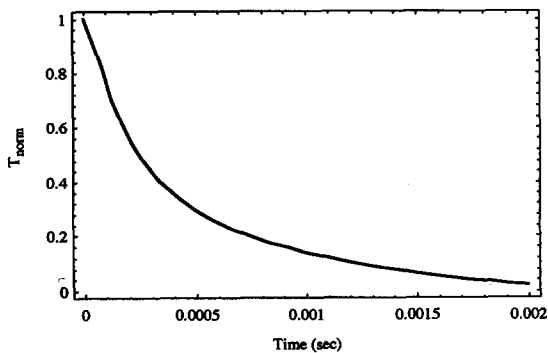$$t_{PD} = \frac{1.4 \times 10^{-3}}{8} = 0.17 \times 10^{-3}\,\text{s}.$$

Fig. 10. Computed normalized temperature $(T_i - T_0)/(T_i - T_0)$ for slab of 200 μm thickness surrounded by copper (simulating simulating hat-shaped specimen).

The cooling time was estimated by a 1D finite difference heat transfer calculation assuming that heat is instantaneously generated in a 200 μm slab and is then allowed to be conducted into a semi-infinite material. The result of such a computation is shown in Fig. 10. The normalized temperature is reduced from T_i to 0.5 T_i in a time, t_c, of

$$t_c = 0.2 \times 10^{-3}\,\text{s}.$$

Thus, the cooling time is of the same order as the deformation time. The very rapid initial drop in temperature shown in Fig. 10 indicates that, in all probability, the microstructures observed in Figs 5–7 are due to plastic deformation, and were not formed subsequent to it. It should be noted that the times for static (3.6×10^3 s) and dynamic (1.7×10^{-4} s) recrystallization differ by 7 orders of magnitude. Nevertheless, the temperature for both recrystallization conditions is reasonably consistent (~ 500 K).

Thus, dynamic recrystallization is the most likely mechanism responsible for the generation of the microcrystalline structure. Derby [33] classified dynamic recrystallization into two types (rotation [or *in situ*] recrystallization and migration recrystallization), and developed a "universal" plot relating the normalized stress level, σ/μ, to a normalized dynamically recrystallized or recovered grain size, d/b, where μ and b are the shear modulus and Burgers vector, respectively. In migration recrystallization, when the strain reaches a critical level, new strain-free grains nucleate and grow within the deforming material. The nucleation frequency, growth mobility, and strain rate establish a steady-state grain size. As noted earlier [10], both Sandstrom and Lagneborg [34] and Derby and Ashby [35] arrive at predictions of the steady-state grain size that are related to the strain rate by

$$d \propto \frac{1}{\dot{\varepsilon}^{1/2}}.$$

In rotation recrystallization, a dynamically recovered substructure undergoes a gradual increase in misorientation, leading to the transformation of cell boundaries into sub-boundaries, and then into high-angle boundaries.

The mechanism of dynamic recrystallization envisaged in the electron micrographs of Figs 5–7 is slightly different from the classical recrystallization mechanisms. Figure 11 is a schematic depiction of the sequence of changes leading to the final recrystallized structure in the shear band. The initial deformation structure produced by shock loading is unstable and, upon plastic deformation breaks down, yielding elongated sub-grains. These elongated sub-grains have a thickness of $\sim 0.1\,\mu$m and a length that exceeds 1 μm. They eventually break down, leading to small recrystallized grains. Once this microcrystalline structure is established, it remains stable by being subjected to migration recrystallization.
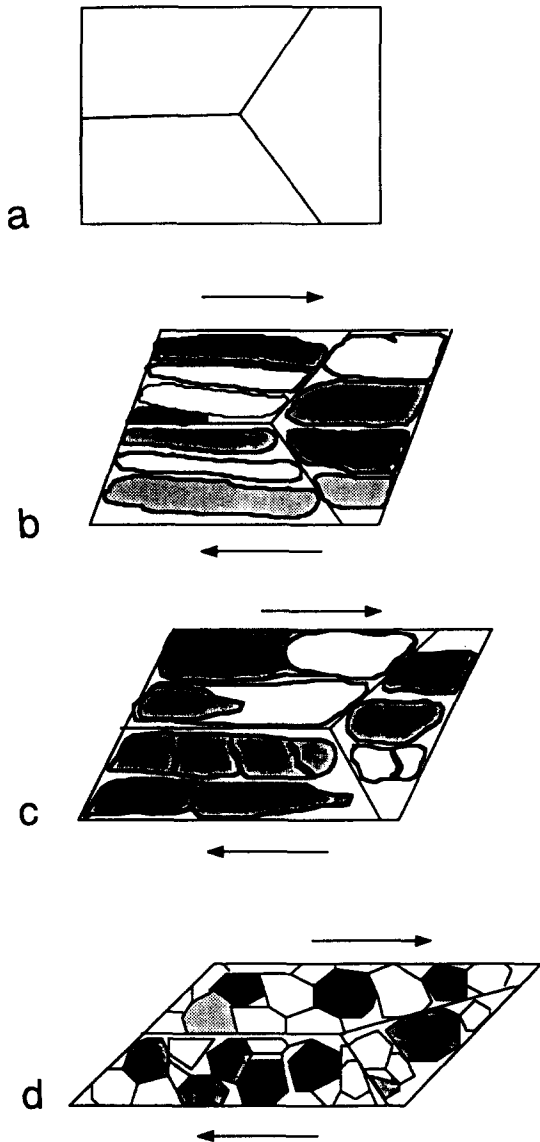
Fig. 11. Schematic representation of observed mechanism of dynamic recrystallization for shock-conditioned copper (a) initial shock-conditioned cell structure; (b) formation of elongated cells and sub-grains by plastic deformation of cell structure; (c) breakup of elongated subgrains at critical strain; (d) final microcrystalline structure.
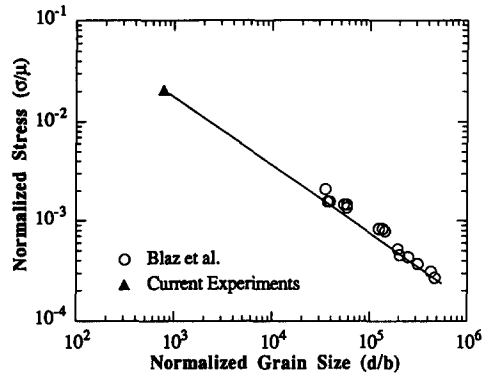

Fig. 12. Normalized grain size as a function of normalized uniaxial normal stress for dynamic recrystallization from Blaz *et al.* [37] and datum point for current experiments.
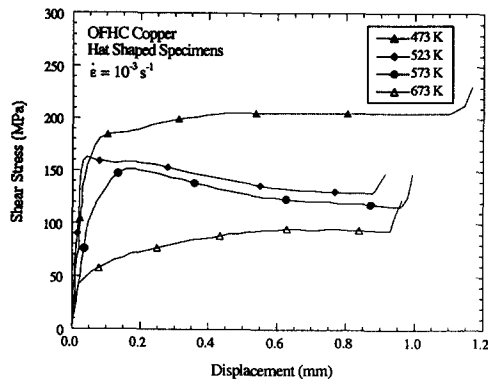

Fig. 13. Shear stress vs. displacement curves for the hat-shaped specimens teated at 10^{-3}/s and different temperatures; notice softening for the 523 and 573 K tests.

The recrystallized grain size observed in the current experiments is smaller, by one order of magnitude, that grain sizes reported in the literature (Jonas *et al.* [36]; Derby [33]). It is therefore instructive to establish whether it is consistent with previous measurements. Blaz *et al.* [37] measured the recrystallized grain size in copper and their results are shown in the σ/μ vs d/b plot of Fig. 12. The following relationship is obeyed

$$\frac{\sigma}{\mu}\left(\frac{d}{b}\right)^m = k.$$

The value of m obtained by Blaz *et al.* [37] is 0.81. The current result is shown in the same plot and is consistent with an extrapolation of the results

by Blaz *et al.* [37]. Derby [33] developed a theory that predicts this response, but it only applied to migration recrystallization.

In order to confirm that dynamic recrystallization occurs in the predicted temperature range, hat-shaped specimens were tested quasi-statically (10^{-3}/s) at varying temperatures. The results, (Fig. 13) show clearly that dynamic recrystallization, identified through a softening in the stress vs displacement curve, was indeed present. Whereas experiments conducted at 423 K and lower temperatures showed work-hardening, the tests conducted at 523 and 573 K show clear evidence of softening. At 673 K, the flow stress is considerably decreased, and the material work hardens again. These experiments were carried out to a displacement of ~1 mm, yielding a shear strain of ~5 (see upturn in plots of Fig. 13). The optical micrographs of the shear deformation region show significant differences compared with the dynamically tested samples. Figure 14(a) shows the band produced at 523 K. The room temperature shear band microstructure (not shown) is rather broad (~300 μm) and its thickness is reduced to ~50 μm at 523 K. Observations at higher magnification reveal profuse recrystallized grains within the band, shown in Fig. 14(b). These recrystallized grains
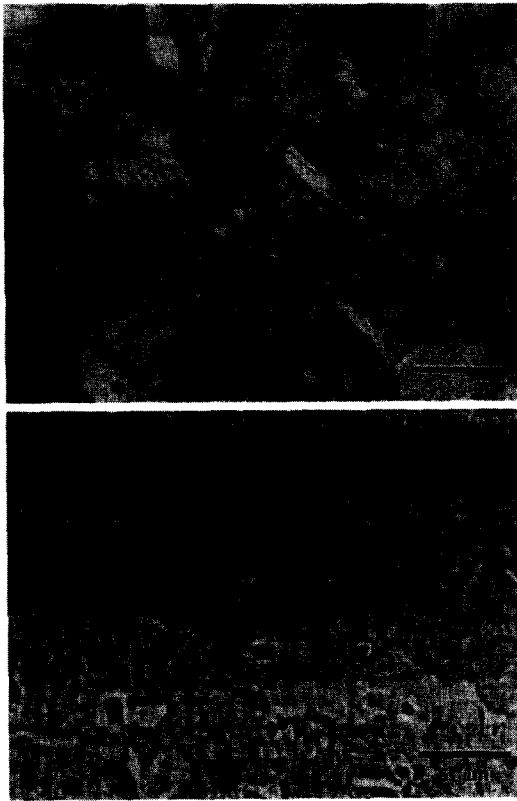
Fig. 14. (a) Optical micrograph of shear localization region in a hat-shaped specimen deformed at 523 K and 10^{-3}/s; notice the dynamic recrystallization that took place. (b) Scanning electron micrograph of same region as (a) showing more clearly the recrystallized grains.

have sizes of $\sim 1.5 \mu$m, in qualitative agreement with the predictions of Sandstrom and Lagneborg [34], Derby and Ashby [35], and Derby [33]. At 673 K, the material has recrystallized prior to mechanical testing and is in the annealed condition. Thus, the localization is much less evident.
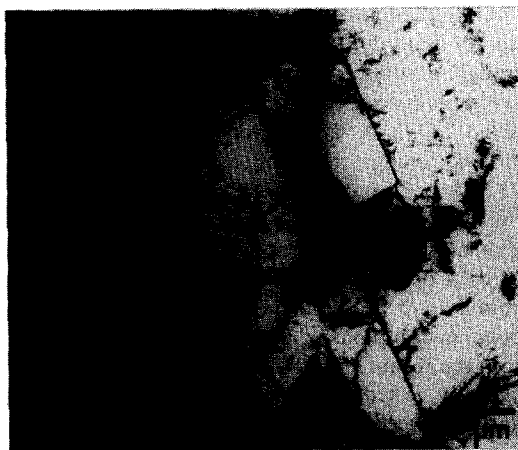

Fig. 15. Transmission electron micrograph of shear localization region in hat-shaped specimen deformed at 523 K and 10^{-3}/s strain rate. Note that the recrystallized grains are several micrometers in diameter; several annealing twins are evident.

The microstructure observed by optical and scanning-electron microscopy in Fig. 14 is revealed in much greater detail by transmission-electron microscopy. Figure 15 shows the microstructure produced by subjecting shocked copper to low-strain-rate deformation in a hat-shaped specimen. The scale of the microstructure shown in Fig. 15 is quite different from that shown in Fig. 7. The morphology and size of the grains produced by the quasi-static plastic deformation are quite different from those generated by high strain rate, with much larger grains which often possess annealing twins produced at the lower strain rate. The grain size is 1–3 μm and several annealing twins are seen, in contrast with Fig. 7. These are freshly formed grains in which subsequent plastic deformation was rather minimal. The dislocation density varied from grain to grain, indicating that the post-deformation quench ensured the retention of the features of plastic deformation. The role played by annealing (or recrystallization) twins in recrystallization has been demonstrated by numerous investigators. Merklen *et al.* [38], Peters [39], Ralph [40], Wilbrandt and Haasen [41], and Rae [42] show clear evidence of the advance of recrystallization regions by the migration of semi-coherent annealing-twin boundaries, which exhibit a much greater mobility than coherent twin boundaries. The presence of annealing (or recrystallization) twins within the recrystallized regions, as evidenced, is a distinct feature of migration recrystallization. Grain boundaries separating the recrystallized regions from the deformed, but unrecrystallized regions often had faceted and irregular shapes, that indicate that the migration process was interrupted and "frozen in" by the post-deformation quench. The observations summarized in Fig. 15 indicate that the process of microstructural evolution in low-strain-rate deformation of pre-heated and pre-shocked copper is one of dynamic recrystallization by migration.

4. CONCLUSIONS

1. Systematic experiments conducted at high strain rates ($\sim 4 \times 10^4 \, s^{-1}$) on copper specimens pre-hardened by shock-wave deformation revealed a microstructure consisting of equiaxed grains (~ 0.1–0.3μm) with a low dislocation density when the imparted plastic shear strain exceeded 2.

2. Plastic deformation was forced into a region with a thickness of ~ 0.2 mm, and therefore post-deformation cooling was sufficiently rapid to ensure, to a reasonable degree of certainty, that the observed microstructure was produced during plastic deformation and not during subsequent cooling.

3. It is proposed that dynamic recrystallization is responsible for the observed microstructure. The recrystallized grain size is consistent with the universal relationship proposed by Derby [33] based on extrapolated results from Blaz *et al.* [37].

4. The two classical dynamic recrystallization mechanisms, migration recrystallization and rotation recrystallization, are compared to the observed microstructures, and it is proposed that a third mixed-mode mechanism operates at high strain rate.

5. Low-strain-rate experiments conducted on the pre-heated specimens revealed, in the temperature range 523–573 K, that dynamic recrystallization produced grains with 1–4 μm diameters, indicating that migration recrystallization occurred.

REFERENCES

1. G. I. Taylor, *Proc. R. Soc. Lond. A* **145**, 362 (1934).
2. A. Seeger, H. Kromüller, S. Mander and H. Trauble, *Phil. Mag.* **6**, 939 (1961).
3. P. B. Hirsch, *Phil. Mag.* **7**, 67 (1962).
4. D. Kuhlmann-Wilsdorf, *Trans. Am. Inst. Min. Engrs* **224**, 1047 (1962).
5. J. Gil Sevillano, P. van Houtte and E. Aernoudt, *Prog. Mater. Sci.* **25**, 69 (1981).
6. L. M. Brown, *Metall. Trans.* **22**, 1693 (1991).
7. J. Harding, in *Impact Loading and Dynamic Behavior of Materials* (edited by C. Y. Chiem, H. D. Kunze and L. W. Meyer), p. 21. DGM-Informationsgesellschaft, Germany (1988).
8. P. S. Follansbee and U. F. Kocks, *Acta metall.* **36**, 81 (1988).
9. F. J. Zerilli and R. W. Armstrong, *J. appl. Phys.* **61**, 1816 (1987).
10. A. H. Chokshi and M. A. Meyers, *Scripta metall mater* **24**, 605 (1990).
11. M. A. Meyers, L. W. Meyer, J. Beatty, U. R. Andrade, K. S. Vecchio and A. H. Chokshi, in *Shock-Wave and High-Strain-Rate Phenomena in Materials* (edited by M. A. Meyers, L. E. Murr and K. P. Staudhammer), p. 529. Marcel Dekker, New York (1992).
12. M. A. Meyers and L. E. Murr, in *Shock Waves and High-Strain-Rate Phenomena in Metals*, pp. 1041–1043, Appendix B. Plenum Press, New York (1981).
13. M. A. Mogilevsky and L. A. Teplyakova, in *Metallurgical Applications of Shock-Wave and High-Strain-Rate Phenomena* (edited by L. E. Murr, K. P. Staudhammer and M. A. Meyers), p. 419. Marcel Dekker, New York (1986).
14. G. T. Gray, III, in *Shock Compression of Condensed Matter* (edited by S. C. Schmidt, J. N. Johnson and L. W. Davison), p. 407 Elsevier, The Netherlands (1983).
15. P. S. De Carli and M. A. Meyers, in *Shock Waves and High-Strain-Rate Phenomena in Metals* (edited by M. A. Meyers and L. E. Murr), p. 341. Plenum Press, New York (1981).
16. G. T. Gray III, in *Shock Waves and High-Strain-Rate Phenomena in Materials* (edited by M. A. Meyers, L. E. Murr and K. P. Staudhammer), p. 899. Marcel Dekker, New York (1991).
17. K.-H. Hartman, H. D. Kunze and L. W. Meyer, in *Shock Waves and High-Strain-Rate Phenomena in Metals* (edited by M. A. Meyers and L. E. Murr), p. 325. Plenum Press, New York (1981).
18. R. J. De Angelis and J. B. Cohen, *J. Metals* **15**, 681 (1979).
19. D. C. Brillhart, R. J. De Angelis, A. G. Preban, J. B. Cohen and P. Gordon, *Trans. Metall. Soc. AIME* **239**, 836 (1967).
20. L. E. Murr, in *Shock Waves and High-Strain-Rate Phenomena in Metals* (edited by M. A. Meyers and L. E. Murr), p. 753. Plenum Press, New York (1981).
21. G. T. Gray III and P. S. Follansbee, in *Impact Loading and Dynamic Behavior of Materials* (edited by C. Y. Chiem, H. D. Kunze and L. W. Meyer), p. 541. DGM-Informations gesellschaft, Germany (1988).
22. P. Feltham and J. D. Meakin, *Phil. Mag.* **2**, 105 (1957).
23. W. H. Gourdin and D. H. Lassila, *Acta metall. mater.* **39**, 2337 (1991).
24. U. R. Andrade, Ph.D. dissertation, Univ. of California, San Diego (1993).
25. G. Regazzoni, U. F. Kocks and P. S. Follansbee, *Acta metall.* **12**, 2865 (1987).
26. R. J. Clifton, *Proc. IUTAM Symp. on Micro-Mechanics of High Velocity Deformation and Fracture*, Tokyo, Japan (1985).
27. W. Tong, R. J. Clifton and J. Huang, *J. Mech. Phys. Solids* **40**, 1251 (1992).
28. C. D. Liu and M. N. Bassim, *Metall. Trans.* **24A**, 361 (1993).
29. L. E. Murr, in *Shock Waves and High-Strain-Rate Phenomena in Metals* (edited by M. A. Meyers and L. E. Murr), p. 607. Plenum Press, New York (1981).
30. J. R. Kelpaczko, *Mater. Sci. Engng* **18**, 121 (1975).
31. G. R. Johnson and W H. Cook, *Proc. 7th Int. Symp. on Ballistics*, ADPA, The Netherlands (1983).
32. E. A. Chojnowski and R. W. Cahn, in *Metallurgical Effects at High Strain Rates* (edited by R. W. Rohde, B. M. Butcher, J. R. Holland and C. H. Karnes), p. 631. Plenum Press, New York (1973).
33. B. Derby, *Acta metall.* **39**, 955 (1991).
34. R. Sandstrom and R. Lagneborg, *Acta metall.* **23**, 387 (1975).
35. B. Derby and M. F. Ashby, *Scripta metall.* **21**, 879 (1987).
36. J. J. Jonas, C. M. Sellars and W. J. McG. Tegart, *Metall. Rev.* **14**, 130 (1969).
37. L. Blaz, T. Sakai, and J. J. Jonas, *Metal Sci.* **17**, 609 (1983).
38. P. Merklen, E. Furubayashi and H. Yoshida, *Trans. Japan. Inst. Metals* **11**, 252 (1970).
39. B. F. Peters. *Metall. Trans.* **4**, 757 (1972).
40. B. Ralph, *J. Physique* **36**, C4-711 (1975).
41. P. J. Wilbrandt and P. Haasen, *Z. Metall.* **71**, 385 (1980).
42. C. M. F. Rae, in *Interface Migration and Control of Microstructure* (edited by C. S. Pande, D. A. Smith, A. H. King and J. Walter), p. 145. ASM, Metals Park, Ohio (1986).